Classification
Physics Abstracts
32.80P — 32.80B — 42.50

Magnetically assisted Sisyphus effect

Olivier Emile (*), Robin Kaiser (**), Christoph Gerz (***), Hartmut Wallis (****), Alain Aspect (**) and Claude Cohen-Tannoudji

Laboratoire de Spectroscopie Hertzienne de l'Ecole Normale Supérieure et Collège de France (*****), 24 rue Lhomond, 75005 Paris, France

(Received 29 October 1992, received in final form 27 August 1993, accepted 30 August 1993)

Résumé . — Cet article présente une étude expérimentale et théorique du refroidissement laser par une onde stationnaire quasi-résonnante en présence d'un champ magnétique transverse faible (Effet Sisyphe Magnétique). Les calculs théoriques ont été développés sur une transition $J_g = 1 \rightarrow J_e = 1$ correspondant à la situation expérimentale que nous avons étudiée sur la transition $2^3S_1 \longleftrightarrow 2^3P_1$ de l'hélium métastable. Dans ce cas, l'effet Sisyphe magnétique a une action opposée à celle du refroidissement Doppler habituel : il produit un chauffage pour un accord du laser en dessous de résonance. La compétition entre l'effet Sisyphe magnétique et le refroidissement Doppler, qui agissent sur des gammes de vitesse différentes, débouche sur de nouveaux effets intéressants, et notamment sur une force présentant un caractère bistable. Nous avons calculé la force totale en fonction de la vitesse en utilisant une approche semi-classique. Nous avons aussi utilisé une seconde approche théorique où l'impulsion atomique est quantifiée, et qui permet d'étudier l'évolution temporelle de la distribution en vitesse. Les résultats théoriques sont ensuite confrontés aux résultats expérimentaux.

Abstract . — This paper presents an experimental and theoretical study of laser cooling in a standing wave in the presence of a small transverse magnetic field (Magnetically Assisted Sisyphus Effect: MASE). The analysis is worked out for a $J_g = 1$ to $J_e = 1$ transition corresponding to the experiment performed on the $2^3S_1 \longleftrightarrow 2^3P_1$ transition of metastable helium. In this situation, MASE has an effect opposed to the usual Doppler cooling effect, i.e. it produces heating for a negative detuning. Depending on the various parameters, the competition between MASE and Doppler cooling, which act on different velocity ranges, leads to interesting new

(*) *Present address* : Faculteit der Natuurkunde en SterrenKunde, De Boelelaan 1081, 1081 HV Amsterdam, The Netherlands.

(**) *Present address* : Institut d'Optique, Université Paris-Sud, B.P. 147, 91403 Orsay Cedex, France.

(***) *Present address* : NIST, Phys A167, Gaithersburg, Maryland 20899, U.S.A.

(****) *Present address* : Institut für Angewandte Physik der Universität Bonn, Wegelerstrasse 8, D-5300 Bonn 1, Germany.

(*****) Associé au CNRS (U.A. 18) et à l'Université Pierre et Marie Curie.

effects, such as a bistable force. The velocity dependence of the total force is calculated, using a semi-classical approach. A second theoretical treatment, where the atomic motion is quantized, is used to study the time evolution of the velocity distribution. The results of these calculations are compared to experimental observations.

1. Introduction.

For atoms with several Zeeman sublevels in the ground state, optical pumping and light shifts can give rise to laser cooling mechanisms much more efficient than Doppler cooling. After the experimental discovery by the NIST group of sub-Doppler temperatures [1], and the confirmation of this effect by other groups [2, 3], it was soon realized that the new cooling mechanisms were associated with large non-adiabatic effects due to the appearance of long internal times (optical pumping) for an atom moving in a laser configuration exhibiting polarization gradients [2, 4]. A particularly simple example of such a cooling mechanism is the "Sisyphus effect" where, as a consequence of strong correlations which exist between the spatial modulation of light shifts and the spatial modulation of optical pumping rates, the multilevel atom moves up in potential hills more than down [5]. Other types of laser cooling mechanisms in polarization gradients have also been investigated [5, 6].

Actually, Sisyphus cooling was first pointed out for a 2-level atom (e, g) moving in an intense standing wave, without any polarization gradient [7]. In such a case, the energies of the two dressed states originating from e and g and the spontaneous emission rates from these dressed states oscillate in space in a correlated way and this gives rise to a Sisyphus cooling. But at low intensity, one of the two dressed states nearly coincides with the ground state g and has a population nearly equal to 1, even at the antinodes of the standing wave. The fact that the population of this dressed state does not change appreciably along the standing wave explains why Sisyphus cooling can be neglected at low intensity for a 2-level atom. The same conclusion holds for an atom with several ground state sublevels in a weak standing wave without polarization gradients. As long as the laser polarization remains the same, the repartition of populations among the ground state sublevels, and the coherences between them, do not change.

In order to get a Sisyphus effect at low intensity and in the absence of polarization gradients, a new perturbation must be added which can change the repartition of the populations among the ground state sublevels. This can be achieved by adding a small transverse static magnetic field $\mathbf{B}_0$. Near the nodes of the standing wave, where the light shifts vanish, $\mathbf{B}_0$ introduces couplings between the degenerate Zeeman sublevels, and a moving atom can experience non adiabatic (Landau-Zener type) transitions between ground state Zeeman sublevels. Then, when the atom arrives near an antinode, optical pumping puts it back in the lowest Zeeman sublevel, so that on the average the atom moves up in potential hills more than down. Such a magnetically assisted Sisyphus effect has been experimentally observed [8-10]. Velocity selective resonances have also been observed in the presence of a static magnetic field [11, 12]. General theoretical treatments have been given in [13]. For a $J_g \longleftrightarrow J_e = J_g + 1$ transition, cooling occurs only for a red detuning between the laser frequency ω_L and the atomic frequency ω_0 ($\omega_L < \omega_0$). For a $J_g \longrightarrow J_e = J_g - 1$ transition, the situation is reversed and Sisyphus cooling has been observed [14] for a blue detuning ($\omega_L > \omega_0$).

The purpose of this paper is to investigate situations where magnetically assisted Sisyphus effect (MASE) exhibits new features [10]. The corresponding experiments have been performed

on metastable He atoms on a $J_g = 1 \longleftrightarrow J_e = 1$ transition. In such a situation, the velocity dependent forces associated respectively with MASE and with Doppler cooling have opposite signs, and the values of the parameters for helium are such that the competition between these two mechanisms leads to spectacular new effects. Another remarkable feature of helium is related to the large recoil velocity (9.2 cm/s); in that case, a full quantum treatment appears to be more convenient and more appropriate for giving a full account of the experimental results than the usual semi-classical description in terms of a mean force and a momentum diffusion coefficient (this was already noticed for the treatment of the Mechanical Hanle Effect of helium [15]).

The paper is organized as follows. We first give in section 2 a qualitative description of MASE, a semi-classical calculation of this effect being outlined in section 3. We then present in section 4 our experimental results, and we discuss them qualitatively in the light of the results of sections 2 and 3. When the transient regime needs to be accounted for, a full quantum treatment is more suitable. Such a treatment is given in section 5 and its predictions are compared with the experimental observations.

2. Qualitative presentation of MASE.

We consider an atomic beam propagating along the Oy axis, and irradiated at right angle by a σ^+ polarized resonant laser standing wave along Oz (Fig. 1). This laser excites a transition

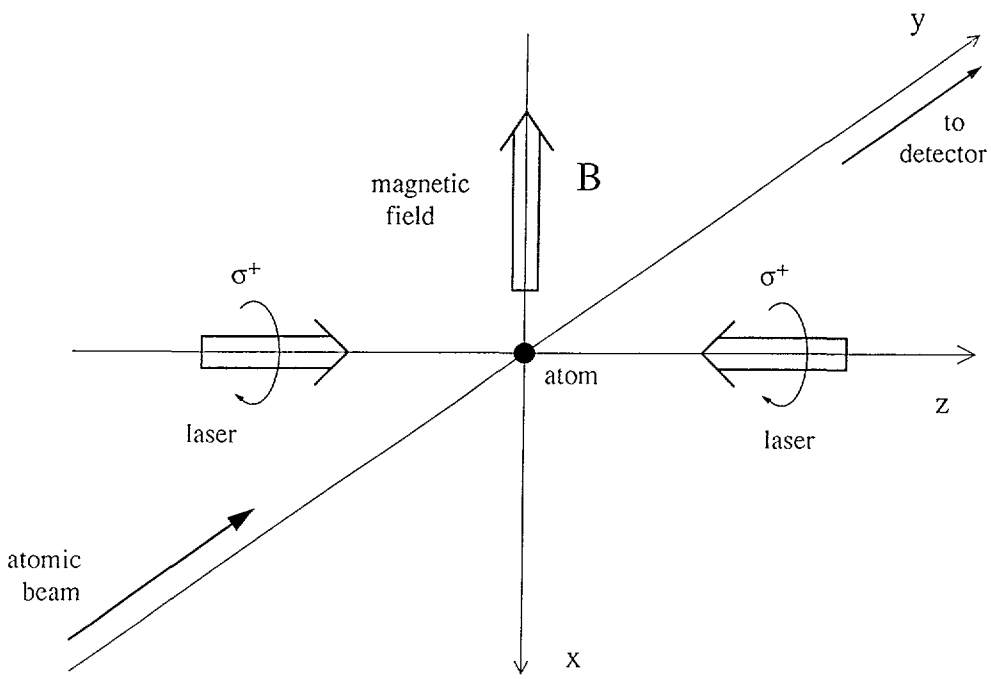

Fig. 1. — Experimental configuration: the laser beam is applied transversely to the atomic beam, and can deflect the atoms. This deflection is measured by a detector which is scanned in the $z-$direction.

$J_g = 1 \longleftrightarrow J_e = 1$, the Clebsch-Gordan coefficients of this transition being given in figure 2. In the absence of magnetic field, the ground state sublevels have their degeneracy removed by the laser excitation, and optical pumping by the σ^+ light transfers all the atomic population in g_+. Since there is no σ^+ transition starting from g_+, the light-shift of g_+ is equal to zero. On the other hand, the two sublevels g_- and g_0 are light-shifted by the same amount since the square of the Clebsch-Gordan coefficients of the two σ^+ transition starting from g_- and g_0 are equal (Fig. 2). Because of the variation of the light intensity along Oz, the light-shifts of g_- and g_0 are spacially modulated, maximum at an antinode and null at a node, as shown in figure 3. We suppose here that the detuning:

$$\delta = \omega_L - \omega_0 \tag{2.1}$$

between the laser frequency ω_L and the atomic frequency ω_0 is negative, so that light shifts in the ground state are negative. An atom travelling in this standing wave is optically pumped into g_+ where it experiences no force because the energy of this sublevel is position independent.

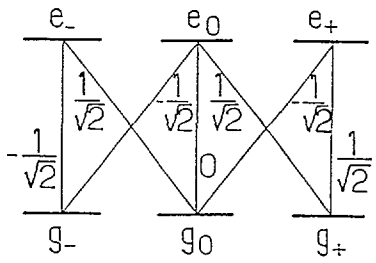

Fig. 2. — Atomic level scheme for observation of MASE with a σ^+ circularly polarized laser. The Zeeman sublevels g_+, g_0, and g_- are taken by reference to the laser beam propagating along Oz. At zero magnetic field, the atoms are optically pumped into g_+ where they no longer interact with the laser. We have indicated the Clebsch-Gordan coefficients characterizing the strength of the transitions.

Suppose now that we apply a weak transverse static magnetic field $\mathbf{B}_0$ along the third axis Ox of figure 1, producing between g_-, g_0 and g_+ off diagonal couplings smaller than the value of the light shift at an antinode. In such a case, the sublevels remain almost unchanged at an antinode, and an atom moving around an antinode is still optically pumped into g_+ where it experiences no force. On the contrary, around a node, the precession induced by $\mathbf{B}_0$ between g_+ and g_0 and between g_0 and g_- is not negligibly small compared to the precession due to light shifts, so that an atom travelling through a node may be found in g_0 or g_- just after the node. Such transfers can also be interpreted as resulting from Landau-Zener type transitions induced by $\mathbf{B}_0$ for an atom moving near a node where the three sublevels are degenerate ([1]). Once the atom has been transferred to the sublevels g_0 or g_- which are spatially modulated, it experiences a force. In the case of figure 3, corresponding to a negative detuning of the laser, the atom is accelerated between the node and the antinode. If the atom remained on the same sublevel, it would then decelerate between the antinode and the following node, and after one period (i.e. half a wavelength) the kinetic energy would remain unchanged. In fact, the circularly polarized laser tends to optically pump back the atom from g_- and g_0 into g_+,

([1]) For the generalization of the Landau Zener formula to the case of two tangent levels see [16].

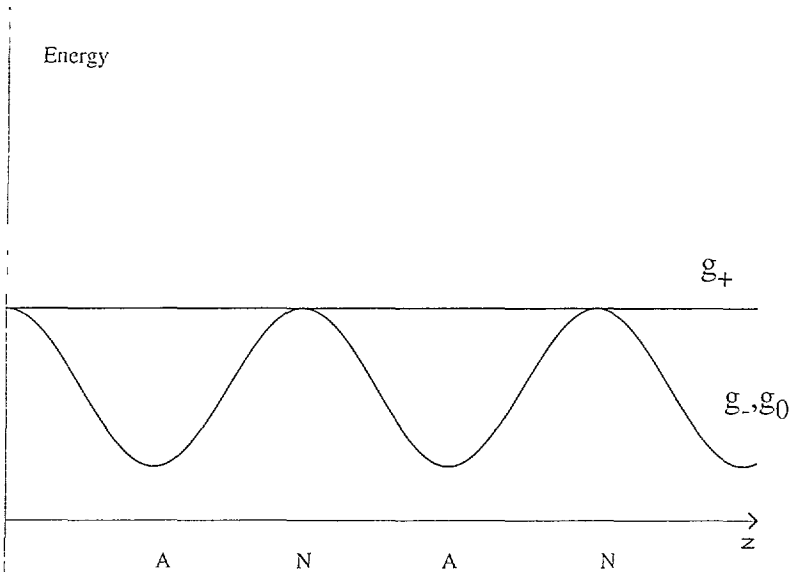

Fig. 3. — Spatial modulation of the 3 ground state sublevels energy with a stationary laser wave σ^+ polarized. The ground states $|g_-\rangle$, $|g_0\rangle$ experience the same light shift, maximum at a node and zero at an antinode. The state $|g_+\rangle$ experiences no light shift because it does not interact with the σ^+ light.

and this is more likely to happen around the antinode, where the laser intensity is maximum. The atom then proceeds on g_+ which is flat. This process is sketched in figure 4, and we see that the net result is an increase of the kinetic energy of the moving atom. For a positive laser detuning, we would have the opposite conclusion: the kinetic energy of the atom would decrease.

The physical mechanism we have just described, and which is also discussed in [8-10], is quite analogous to the Sisyphus effect occurring for a multilevel atom moving in a laser configuration with a polarization exhibiting a gradient of ellipticity [5]. In the case presented here, the magnetic field plays an essential role [8-14], and this is why such an effect may be called Magnetically Assisted Sisyphus Effect. Like for any kind of Sisyphus effect, it would be possible to show that the corresponding force varies linearly with the velocity v around $v = 0$. However, there is here a striking difference: the sign of the effect is not the usual one [5, 6] since we have here a heating force (the force increases with the velocity) for a negative detuning, and a cooling force for a positive detuning. This different sign has dramatic consequences on the behavior of the force as a function of velocity, when one does not restrict the study to very small velocities. Indeed, it is well-known [5] that Sisyphus cooling is efficient only at velocities smaller than a critical velocity v_S. This velocity is such that the atom travels a distance on the order of a fraction of a wavelength $(2\pi/k_L)$ during $(\Gamma')^{-1}$ (which is the optical pumping time from g_- to g_+). This critical velocity can thus be defined by:

$$v_S = \Gamma'/k_L \tag{2.2}$$

When the atomic velocity is larger than v_S, the Sisyphus force gets smaller, while the absorption process becomes more sensitive to the atomic velocity: because of the Doppler effect, the

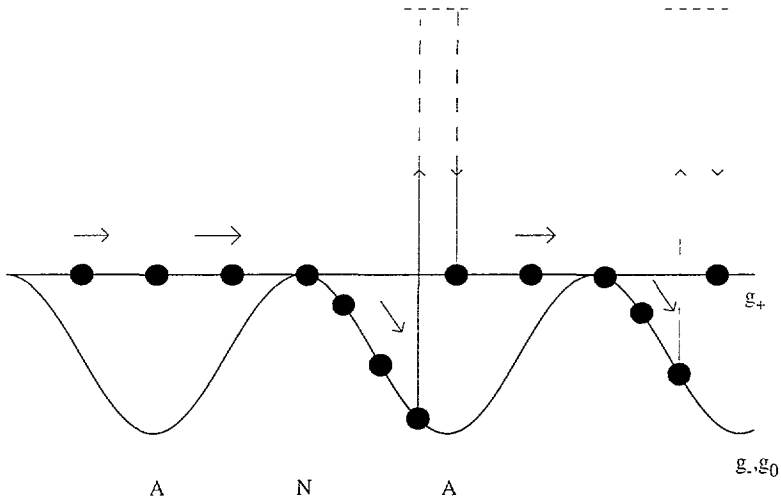

Fig. 4. — MASE for a $J_g = 1$ to $J_e = 1$ transition in the case of a negative detuning. When an atom travels through a node, it experiences a precession because of the transverse magnetic field, and it can leave the region in the $|g_0\rangle$ or even $|g_-\rangle$ sublevel. There it is accelerated, until it is optically pumped to g_+ where it has a uniform motion. The process can resume at the next node, and the net result is an increase of the kinetic energy of the atom.

probabilities of excitation by the two counterpropagating waves forming the standing wave are no longer equal. The result is the usual Doppler cooling force, which is efficient on a velocity range on the order of v_D, defined by:

$$v_D = \Gamma/k_L \tag{2.3}$$

(note that v_D is larger than v_S since Γ' is smaller than Γ). This Doppler force produces a cooling for a negative detuning, and a heating for a positive detuning. The Doppler force, dominant at large velocities, has thus a sign opposite to that of the Sisyphus force, dominant at low velocity (while in the usual cases the two effects have the same sign and just add up). Note that there are other cases where the Doppler and sub-Doppler forces have opposite signs, for example, the case of a $\sigma^+ - \sigma^-$ configuration (with no **B**-field) for $J_g = J \longrightarrow J_e = J$ and $J_g = J \longrightarrow J_e = J - 1$ transitions when $J > 1$.

In order to get a qualitative understanding of the physical consequences of such a situation, we just add these two forces. We first consider the Doppler force in the typical situation of a detuning $\delta = -\Gamma/2$: it is the sum of two opposite Lorentzian curves centered at $\pm v_D/2$, which gives a curve with a negative slope around $v = 0$. As for the Sisyphus force, we model it by the expression [5]:

$$F_S = \frac{\alpha v}{1 + v^2/v_c^2} \tag{2.4}$$

with v_c of the order of v_S, i.e. smaller than v_D. This curve has a positive slope around $v = 0$, and it has a narrower width. Figure 5 shows the result of this addition. The total force vanishes not only at $v = 0$, but also at $v = +v_1$ and $v = -v_1$, so that there are three "equilibrium" points in velocity space. For a negative detuning (Fig. 5), the two points $v = +v_1$ and $v = -v_1$ are stable, while $v = 0$ is unstable (this results from the sign of the slope around each point). If we let an ensemble of atoms evolve under the effect of such a force, we thus expect that the atoms will get bunched around v_1 and $-v_1$, giving rise to a velocity distribution exhibiting two

bumps, the width of which is determined by the unavoidable fluctuations of the force around its average value (momentum diffusion due to the random character of momentum exchanges between atoms and light).

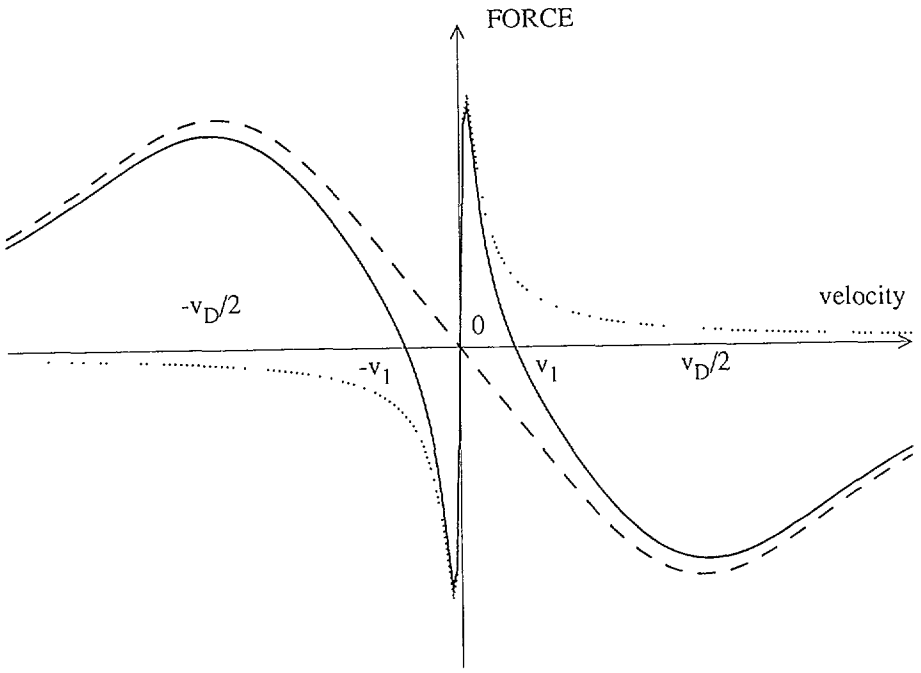

Fig. 5. — Addition of a Sisyphus type force (dotted line) and of a Doppler cooling force (dashed line). Since the two forces have opposite signs, and since they act on different velocity ranges, the resulting curve (full line) crosses the v axis on three points. The two points at $v = v_1$ and $v = -v_1$ are stable equilibrium points, while $v = 0$ is unstable.

In the case of a positive detuning, we expect a force with the same shape but a reversed sign. The physical consequences are then completely different since we have now only one stable point around $v = 0$, and two unstable points at $v = v_1$ and $v = -v_1$. Atoms initially distributed in the interval $[-v_1, v_1]$ will thus be "attracted" towards $v = 0$, whereas atoms with $v > v_1$ or $v < -v_1$ are expelled out. We thus expect a final velocity distribution exhibiting a single bump around zero. Strictly speaking, in such a case, there is no real steady-state distribution since there is a diffusion process in velocity space, allowing atoms to "jump" beyond the values v_1 or $-v_1$, so that they eventually escape. However, provided that this escape mechanism has a characteristic time longer than the bunching time, it should be possible to observe a "metastable" situation with atoms bunched around $v = 0$.

3. Semi-classical calculation of the mean force.

3.1 PRINCIPLE OF THE CALCULATION. — This section is devoted to a calculation of the mean force experienced by an atom moving in a laser standing wave along Oz (Fig. 1). We will use a semi-classical approach, which is valid when the extension of the atomic wave packet is sufficiently small both in position and momentum space [17]. Such a semi-classical approach is now well-known and is discussed in detail in several places [13, 17, 18]. In order to have a self-contained paper, we sketch here the main steps of the calculation.

The mean radiative force can then be written as

$$f(z) = -\left\langle \frac{\partial}{\partial z} V_{\mathrm{AL}}(z) \right\rangle \tag{3.1}$$

Where

$$V_{\mathrm{AL}} = -\mathbf{d} \cdot \mathbf{E}(z) \tag{3.2}$$

is the electric dipole interaction Hamiltonian, describing the coupling between the atomic dipole moment $\mathbf{d}$ and the laser electric field $\mathbf{E}(z)$.

Since the quantum average of expression (3.1) evaluated at the atomic position involves only the internal degrees of freedom, it can be expressed in terms of the atomic density matrix σ describing the internal atomic state. In order to calculate σ, we will use the optical Bloch equations which describe the time evolution of σ, including the Hamiltonian evolution in the external laser and magnetic fields, as well as the damping due to spontaneous emission.

We suppose here that the atom is moving along Oz with a constant velocity v in the laser standing wave. We can thus calculate the density matrix in the forced regime, using a Fourier series expansion. The corresponding equations are solved using the continued fraction method [18].

3.2 SIMPLIFIED LEVEL SCHEME AND CORRESPONDING HAMILTONIAN — We restrict this calculation to situations where the magnetic coupling between the Zeeman sublevels is small compared to the atom-light coupling and to the natural width Γ of the excited state e. With the σ^+ laser polarization considered here, most of the atomic population is concentrated in the three sublevels $|\mathrm{g}_0\rangle = |\mathrm{g}, m_z = 0\rangle$, $|\mathrm{g}_+\rangle = |\mathrm{g}, m_z = +1\rangle$, $|\mathrm{e}\rangle = |\mathrm{e}, m_z = +1\rangle$ (see Fig. 2).

In order to simplify the calculation of this section, we only take into account these three most populated sublevels. The total Hamiltonian H describing the atom in the external laser and magnetic fields can then be written:

$$H = \hbar\omega_0 |\mathrm{e}\rangle\langle\mathrm{e}| + V_B + V_{\mathrm{AL}} \tag{3.3}$$

where $\hbar\omega_0$ is the internal energy interval between e and g, where the atom-laser coupling V_{AL} is given in (3.2), and where

$$V_B = \hbar \frac{\Omega_B}{\sqrt{2}} |\mathrm{g}_0\rangle\langle\mathrm{g}_+| + \mathrm{h.c.} \tag{3.4}$$

describes the Zeeman coupling between g_0 and g_+ due to a transverse static magnetic field applied along Ox (note that Ω_B includes the Landé factor of the ground state). With this notation we get $\Omega_B = 1.75\Gamma$ for $B = 1$ G. In order to reexpress V_{AL} in a form similar to (3.4), we start from the expression of the electric field of a σ^+ laser standing wave.

$$\mathbf{E}(z,t) = \mathcal{E}^+(z) \mathrm{e}^{-i\omega_{\mathrm{L}} t} + \mathrm{c.c.} \tag{3.5}$$

where the positive frequency component $\mathcal{E}^+(z)$ can be written:

$$\mathcal{E}^+(z) = \mathcal{E}_0 \left(\frac{\mathbf{e}_x + i\mathbf{e}_y}{\sqrt{2}} \right) \cos kz \tag{3.6}$$

Inserting (3.6) into (3.2) and using the rotating wave approximation, we get:

$$V_{\mathrm{AL}} = \frac{\hbar\Omega_{\mathrm{L}}}{2} \cos kz \left[|\mathrm{e}\rangle \langle \mathrm{g}_0| \, \mathrm{e}^{-i\omega_{\mathrm{L}}t} + \mathrm{h.c.} \right] \tag{3.7}$$

where

$$\Omega_{\mathrm{L}} = -2\langle \mathrm{e}|\mathbf{d} \cdot \frac{\mathbf{e}_x + i\mathbf{e}_y}{\sqrt{2}} |\mathrm{g}_0\rangle \, \mathcal{E}_0/\hbar \tag{3.8}$$

is the Rabi frequency characterizing the atom-laser coupling at an antinode.

3.3 OPTICAL BLOCH EQUATIONS. — The density matrix evolution is determined from the optical Bloch equations

$$\frac{\mathrm{d}\sigma}{\mathrm{d}t} = \frac{1}{i\hbar}[H, \sigma] + \left(\frac{\mathrm{d}\sigma}{\mathrm{d}t} \right)_{sp} \tag{3.9}$$

where $(\mathrm{d}\sigma/\mathrm{d}t)_{\mathrm{sp}}$ represents the relaxation terms due to spontaneous emission.

From (3.3), (3.4), (3.7) and (3.9), we deduce a set of coupled linear differential equations:

$$\frac{\mathrm{d}\sigma_{\mathrm{g_0g_0}}}{\mathrm{d}t} = \frac{i\Omega_B}{\sqrt{2}} \left(\sigma_{\mathrm{g_0g_+}} - \sigma_{\mathrm{g_+g_0}} \right) + \frac{i\Omega_{\mathrm{L}}}{2} \cos kz \left(\tilde{\sigma}_{\mathrm{g_0e}} - \tilde{\sigma}_{\mathrm{eg_0}} \right) + \frac{1}{2}\Gamma\sigma_{\mathrm{ee}} \tag{3.10.a}$$

$$\frac{\mathrm{d}\sigma_{\mathrm{g_+g_+}}}{\mathrm{d}t} = \frac{i\Omega_B}{\sqrt{2}} \left(\sigma_{\mathrm{g_+g_0}} - \sigma_{\mathrm{g_0g_+}} \right) + \frac{1}{2}\Gamma\sigma_{\mathrm{ee}} \tag{3.10.b}$$

$$\frac{\mathrm{d}\sigma_{\mathrm{ee}}}{\mathrm{d}t} = \frac{i\Omega_{\mathrm{L}}}{2} \cos kz \left(\tilde{\sigma}_{\mathrm{eg_0}} - \tilde{\sigma}_{\mathrm{g_0e}} \right) - \Gamma\sigma_{\mathrm{ee}} \tag{3.10.c}$$

$$\frac{\mathrm{d}\sigma_{\mathrm{g_0g_+}}}{\mathrm{d}t} = \frac{i\Omega_B}{\sqrt{2}} \left(\sigma_{\mathrm{g_0g_0}} - \sigma_{\mathrm{g_+g_+}} \right) - \frac{i\Omega_{\mathrm{L}}}{2} \cos kz \, \tilde{\sigma}_{\mathrm{eg_+}} \tag{3.10.d}$$

$$\frac{\mathrm{d}\tilde{\sigma}_{\mathrm{g_0e}}}{\mathrm{d}t} = -\frac{i\Omega_B}{\sqrt{2}} \left(\tilde{\sigma}_{\mathrm{g_+e}} \right) + \frac{i\Omega_{\mathrm{L}}}{2} \cos kz \left(\sigma_{\mathrm{g_0g_0}} - \sigma_{\mathrm{ee}} \right) - \left(\frac{\Gamma}{2} + i\delta \right) \tilde{\sigma}_{\mathrm{g_0e}} \tag{3.10.e}$$

$$\frac{\mathrm{d}\tilde{\sigma}_{\mathrm{g_+e}}}{\mathrm{d}t} = -\frac{i\Omega_B}{\sqrt{2}} \tilde{\sigma}_{\mathrm{g_0e}} + \frac{i\Omega_{\mathrm{L}}}{2} \cos kz \, \sigma_{\mathrm{g_+g_0}} - \left(\frac{\Gamma}{2} + i\delta \right) \tilde{\sigma}_{\mathrm{g_+e}} \tag{3.10.f}$$

Where

$$\tilde{\sigma}_{\mathrm{eg_i}} = \exp\left(i\omega_{\mathrm{L}}t\right) \sigma_{\mathrm{eg_i}} \qquad \text{with} \qquad i = 0, + \tag{3.11}$$

and three other equations, complex conjugate of (3.10.d-f)

3.4 DENSITY MATRIX IN THE FORCED REGIME. — Using now $z = vt$, and neglecting the transient regime, we can write

$$\frac{\mathrm{d}\sigma}{\mathrm{d}t} = v\frac{\mathrm{d}\sigma}{\mathrm{d}z} \tag{3.12}$$

which allows us to transform the equations (3.10) into a set of linear differential equations depending only on z. Using the conservation of the total population $\left(\sigma_{\mathrm{ee}} + \sigma_{\mathrm{g_+g_+}} + \sigma_{\mathrm{g_0g_0}} = 1\right)$,

we transform the 9 homogeneous equations into 8 inhomogeneous ones which can be written in operator form:

$$v\frac{\mathrm{d}\sigma}{\mathrm{d}z} = A\sigma + B \tag{3.13}$$

Since the coefficients appearing in A and B are either constant or proportional to cos kz, we can use a decomposition:

$$A = \frac{A^1}{2}\left(\mathrm{e}^{\imath kz} + \mathrm{e}^{-\imath kz}\right) + A^0 \tag{3.14}$$

$$B = \frac{B^1}{2}\left(\mathrm{e}^{\imath kz} + \mathrm{e}^{-\imath kz}\right) + B^0 \tag{3.15}$$

Taking into account the periodicity of A and B, we look for a periodic solution of equation (3.13) in the form of a Fourier series:

$$\sigma = \sum_{n\in\mathbb{Z}} \sigma^{(n)}\mathrm{e}^{\imath nkz} \tag{3.16}$$

Inserting (3.16) into (3.13) and using (3.14) and (3.15), we get a recursion relation for the Fourier coefficients

$$\begin{aligned} inkv\ \sigma^{(n)} =& A^0\sigma^{(n)} + \frac{A^1}{2}\left(\sigma^{(n+1)} + \sigma^{(n-1)}\right) \\ &+ \frac{B^1}{2}\left(\delta_{n,1} + \delta_{n,-1}\right) + B^0\delta_{n,0} \end{aligned} \tag{3.17}$$

Considering $\sigma^{(n)}$ as a series of vectors in the Liouville space, we define G_n by:

$$\sigma^{(n)} = G_{n-1}\sigma^{(n-1)} \qquad \text{with} \qquad n \geq 2. \tag{3.18}$$

With this definition, the recursion relation (3.17) gives:

$$G_{n-1} = \left[\left(inkv - A^0\right) - \frac{A^1}{2}G_n\right]^{-1}\frac{A^1}{2} \tag{3.19}$$

which can be solved numerically by the continued fractions method generalized for matrices. The corresponding solution for G_1 is:

$$G_1 = \cfrac{1}{\left(2ikv - A^0 - \cfrac{A^1}{2}\cfrac{1}{\left(3ikv - A^0 - \cfrac{A^1}{2}\cdot\right)}\cfrac{A^1}{2}\right)}\frac{A^1}{2} \tag{3.20}$$

G_1 can be then numerically calculated for a given v. Writing then equation (3.17) for $n = 1, -1, 0$, and substituting $G_1\sigma^{(1)}$ for $\sigma^{(2)}$ we get a set of linear equations containing B^1 and B^0. The solution of these equations yields numerical values for $\sigma^{(0)}, \sigma^{(1)}$ and $\sigma^{(-1)}$ for a given set of parameters.

3.5 MEAN FORCE. — We now have to calculate the mean force given by expression (3.1). Because the force varies when the atom moves from a node to an antinode of the standing wave, we average the force over one wavelength. This average depends only on $\sigma^{(1)}$ and we get:

$$f = \hbar k \Omega_{\mathrm{L}} \mathrm{Im}\left(\tilde{\sigma}^{(1)}_{\mathrm{ge}}\right) \tag{3.21}$$

For a given detuning and a given laser coupling, at a fixed velocity, we thus obtain the average force experienced by an atom. Changing v allows us to calculate the average force f as a function of the velocity, for a given set of parameters (laser detuning and intensity, value of the transverse magnetic field). Results of calculations of this type will be presented in section 4, in order to interpret the experimental results. As an example, we present in figure 6a the results of a calculation corresponding to the qualitative discussion of section 2: the magnetic coupling ($\Omega_B = 0.038\Gamma$) is small compared to the natural width Γ of the excited state and to the atom-light coupling at the antinodes ($\delta = -0.94\Gamma$, $\Omega_{\mathrm{L}} = 2.4\Gamma$ at the antinodes, corresponding to a light shift of 0.79Γ, and to an optical pumping rate $\Gamma' \simeq 0.7\Gamma$).

The result of the calculation clearly shows the features predicted by the qualitative discussion. There is a broad structure (width of the order of a few $v_{\mathrm{D}} = \Gamma/k$) corresponding to Doppler cooling. For small velocities (less than $v_{\mathrm{S}} = \Gamma'/k$) there is a strong heating effect due to MASE. As a result of these two competing effects, the force cancels at two stable points, $+v_1$ and $-v_1$ ($v_1 \simeq 5.2\hbar k/M$).

3.6 CALCULATION WITH 6 SUBLEVELS. — The calculation above, done with the simplified 3 sublevels scheme introduced in subsection 3.2, can in fact be easily generalized for taking into account all the 6 sublevels of the transition. It requires more computer power, since the density matrix has 36 elements instead of 9, but all the steps of the calculation are exactly the same. Note that the calculation is now more precise (within the framework of the semi-classical description). In particular, the Zeeman effect in the excited state is correctly taken into account, as well as the possibility for the atoms to precess to the $(\mathrm{g}, m_z = -1)$ Zeeman sublevel when crossing an antinode where the magnetic field plays the predominant role.

Figure 6b presents the results of this complete calculation, for the same parameters as the one of the approximate calculation of figure 6a. Although the results are quite similar, we can note slight differences: the maximum value of the heating force is slightly larger ($0.63\hbar k\Gamma/2$ instead of $0.60\hbar k\Gamma/2$), and we observe a similar feature for the maximum cooling force. These effects can be attributed to the fact that atoms precessing to the $(\mathrm{g}, m_z = -1)$ Zeeman sublevel exchange more photons before being optically pumped into $(\mathrm{g}, m_z = +1)$. Note however that the values of the zeros of the force, $\pm v_1$, are essentially unchanged.

To conclude this section, we see that the simplified description in terms of 3 sublevels is quite reliable. But if precise quantitative results are required, it is necessary to make the calculation with the complete system of levels.

4. Experimental results — Qualitative discussion.

4.1 EXPERIMENTAL SET-UP. — The experimental set-up (see Fig. 7) is the same as the one described in [15, 19-21]. Metastable helium atoms from a collimated supersonic beam interact with the light field. Their transverse velocity distribution is then determined from their deflection as measured by a scanned electron multiplier. With the beam source cooled to liquid nitrogen temperature, the longitudinal velocity distribution peaks at 1300 m/s and has a width δv of 150 m/s (HWHM). Collinear electron bombardment excites the atoms to various

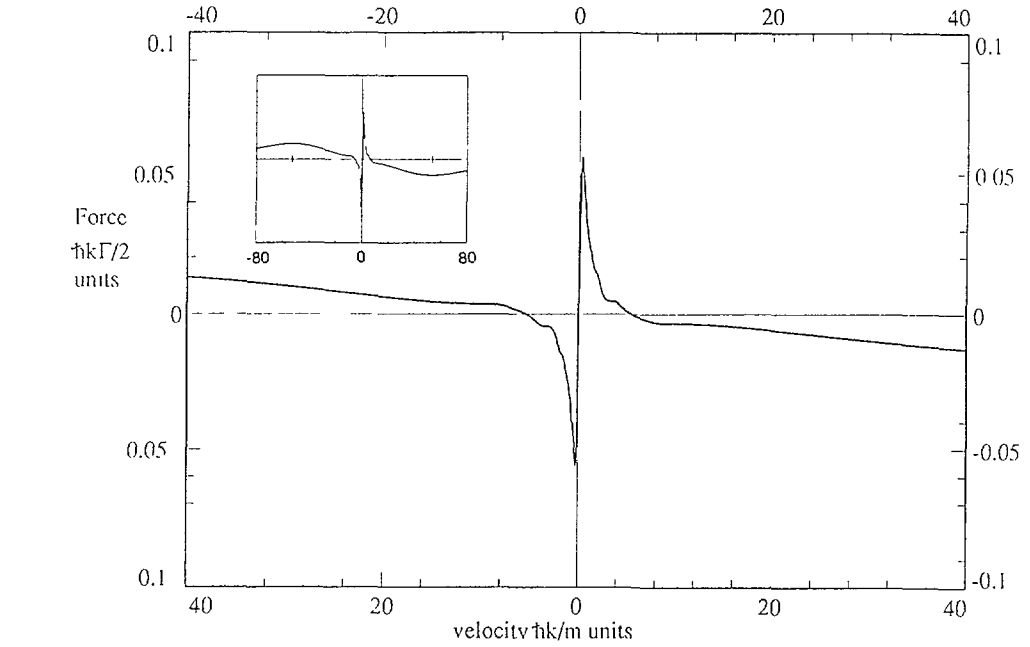

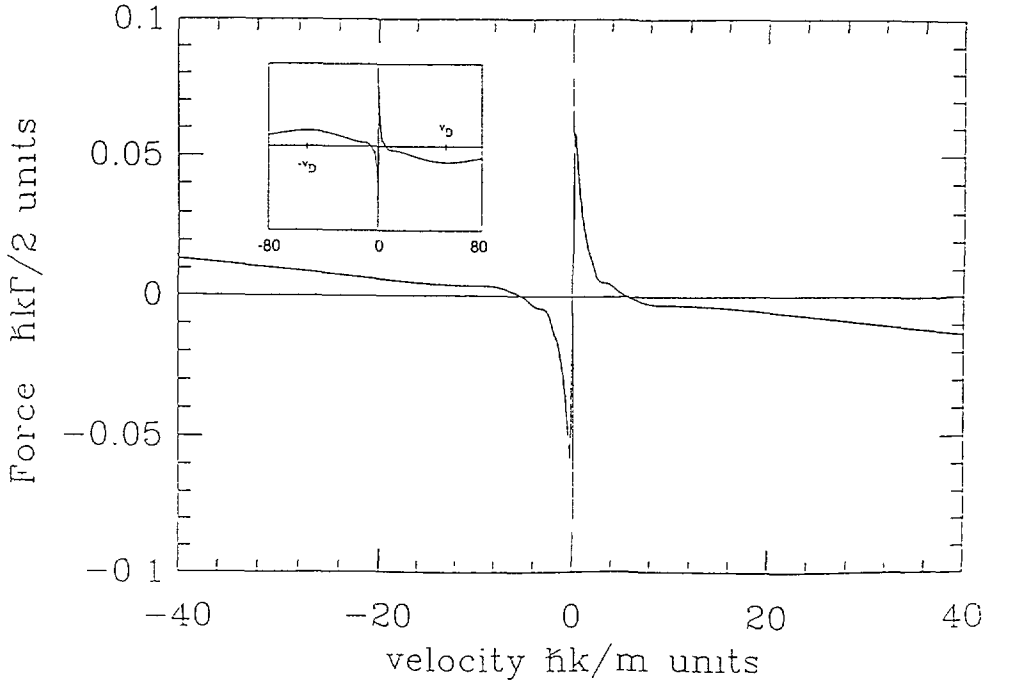

Fig. 6. — Result of a semi-classical calculation of the average force as a function of the atomic velocity, by a continued fraction expansion. The selected parameters ($\Omega_B = 0.038\Gamma$, $\Omega_L = 2.4\Gamma$, $\delta = -0.94\Gamma$) correspond to the qualitative discussion of section 2, i.e. we expect a heating due to MASE at small velocities, and a Doppler cooling at large velocities, with two stable points at $\pm\ v_1$. a) corresponds to a calculation done with the simplified 3-levels scheme of section 3.2. b) corresponds to an exact calculation involving all the 6 sublevels: the results are very similar, but absolute values of the force are slightly larger. In the inset, we have plotted the force from $-80\hbar k$ to $+80\hbar k$. (The vertical scale can be inferred from the main plot).

metastable states. Light from a helium discharge lamp empties the singlet states, so that only atoms in the 2^3S_1 state survive.

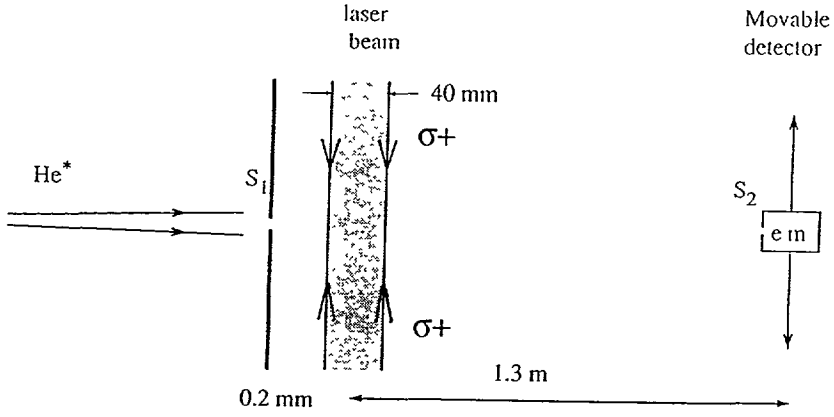

Fig. 7. — Experimental set-up. The metastable beam of helium, transversely limited by slit s_1 (0.2 mm wide), is analyzed by an electron multiplier with a similar slit s_2 yielding the transverse velocity profile. When the laser beam is applied, the transverse velocity profile is modified.

The atoms interact with a circularly polarized transverse standing wave, with a frequency ω_L tuned to the $2^3S_1 - 2^3P_1$ transition ($\lambda = 1.083$ μm; natural linewidth $\Gamma/2\pi = 1.6$ MHz). The home built LNA laser [21] is frequency stabilized to 0.4 MHz and locked to the $2^3S_1 - 2^3P_1$ line by saturated absorption in a He RF-discharge cell. Two Helmholtz coils around the cell allow one to detune the laser frequency by applying a magnetic field in the cell. The laser beam used for the interaction with the atoms is enlarged (and limited by a baffle) in order to have an almost uniform intensity in the interaction region 39 mm long. The corresponding interaction time is then 30 μs, i.e. $300\Gamma^{-1}$ The standing wave is obtained by retroreflecting the σ^+ polarized laser on a mirror. The intensity (of one travelling wave) adjusted by the use of neutral density filters is typically on the order of 0.9 mW/cm^2, corresponding to a Rabi frequency at an antinode of $\Omega_L = 2.4\Gamma$ (as defined in Eq. (3.8)).

The magnetic field in the interaction region is controlled by three pairs of coils, approximately in the Helmholtz position, so that the applied field is homogeneous to better than 10^{-3} in the interaction volume. These coils are placed along Ox, Oy and Oz respectively; we can thus apply a magnetic field along the axis of propagation of the laser (Oz), or transverse to it (Ox and Oy).

In order to define the velocity distribution along the axis of propagation of the laser beams (Oz), we limit the atomic beam by a slit 0.2 mm wide, placed just before the interaction region. The atomic beam profile is scanned along Oz by an electron multiplier with a similar input slit, placed 1.3 m after the interaction region. This detector is sensitive only to the metastable atoms. Because of the narrow longitudinal velocity distribution (along Oy), we obtain directly the velocity distribution along Oz, with a resolution of 0.13 m/s (HWHM) in the range $\pm$ 2 m/s. Comparing these profiles with and without the lasers allows us to observe the force acting on the atoms.

4.2 TYPICAL FEATURES OF MASE: OBSERVATION AND INTERPRETATION.

4.2.1 *Negative detuning.* — In this section, we present results obtained in a situation corresponding to the qualitative discussion of section 2, and to the calculations of section 3. The first result is shown in figure 8a. It corresponds to a negative detuning, with the parameters selected for the calculation of figure 6. The velocity distribution after interaction with the light presents the expected double bump structure, with a hole around $v = 0$ corresponding to the heating effect of MASE when δ is negative. The positions of the maxima of the bumps ($v = \pm\ 4.7\hbar k/M$) are slightly different from the position of the stable zeros of $F(v)$ ($v_1 = \pm\ 5.3\hbar k/M$), but within the precision of the experimental data ($0.5\hbar k/M$).

Figure 8b presents the influence of the interaction time on the velocity distribution. It has been obtained by using various masks of increasing width placed in the interacting laser beam. It clearly appears that the transient evolution plays a major role, and that the steady state situation is not completely reached at $t = 300\Gamma^{-1}$. We can compare this time scale with the characteristic evolution time of an atom that would be submitted to the force $F(v)$ shown in figure 6. Linearizing around $v = 0$, one finds an exponential evolution of the velocity with a time constant $10\Gamma^{-1}$ (inverse of the slope of $F(v)$ around $v = 0$). A similar procedure around the values $\pm\ v_1$ (stable zeros of $F(v)$) leads to an exponential damping of the velocity with a time constant $300\Gamma^{-1}$. Although the real evolution of the velocity distribution depends on more parameters than the one discussed here, we can conclude that the evolution of the velocity distribution has a transient regime certainly longer than $300\Gamma^{-1}$, if it is due to the force $F(v)$ of figure 6.

A detailed quantitative interpretation of the experimental results, which do not correspond to the steady state situation, would thus require calculating the transient evolution of the velocity distribution. This will be discussed below (Sects. 4.4 et 5.3).

4.2.2 *Positive detuning.* — We show in figure 9a the final velocity distribution obtained with a positive detuning. Figure 9b presents the result of the calculation of the average force in this situation ($\delta > 0$). It predicts a strong cooling around $v = 0$, which is responsible for the central peak in figure 9a, and a weak heating at larger velocities ([2]). As in section 4.2.1, the comparison between the experimental results and the calculation of figure 9b requires to take into account the fact that the steady situation has not yet been reached at the end of the interaction time ($300\Gamma^{-1}$). At this time scale, the MASE cooling around $v = 0$ has already a clear effect, while the heating and diffusion in the wings has not yet produced a significant effect. Note that in this case, as already mentioned in section 2, the peak around $v = 0$ should eventually vanish at very long interaction time, because the atoms diffuse out of the cooling zone $[-v_1, v_1]$.

4.3 OTHER INTERESTING SITUATIONS.

— We present now some results obtained in situations different from the one considered for the discussion of section 2. However, we will see that the experimental data can still be interpreted with qualitative arguments as well as from the calculations of section 3.

4.3.1 *Large transverse magnetic field.* — Consider a situation where the magnetic field is large enough so that the Zeeman shifts are much larger than the light shifts. The qualitative

([2]) The oscillations which appear in the theoretical curve of figure 9b (as well as in Figs. 10b, 11b and, to a smaller extent, in Fig. 6), can be interpreted as resulting from interferences between the contributions of successive Landau Zener transitions. Our experimental resolution does not allow us to observe such structures. Resonances of this type have already been predicted [18, 13] and observed [11, 22, 23] ; for a general review on this type of resonances see [24].

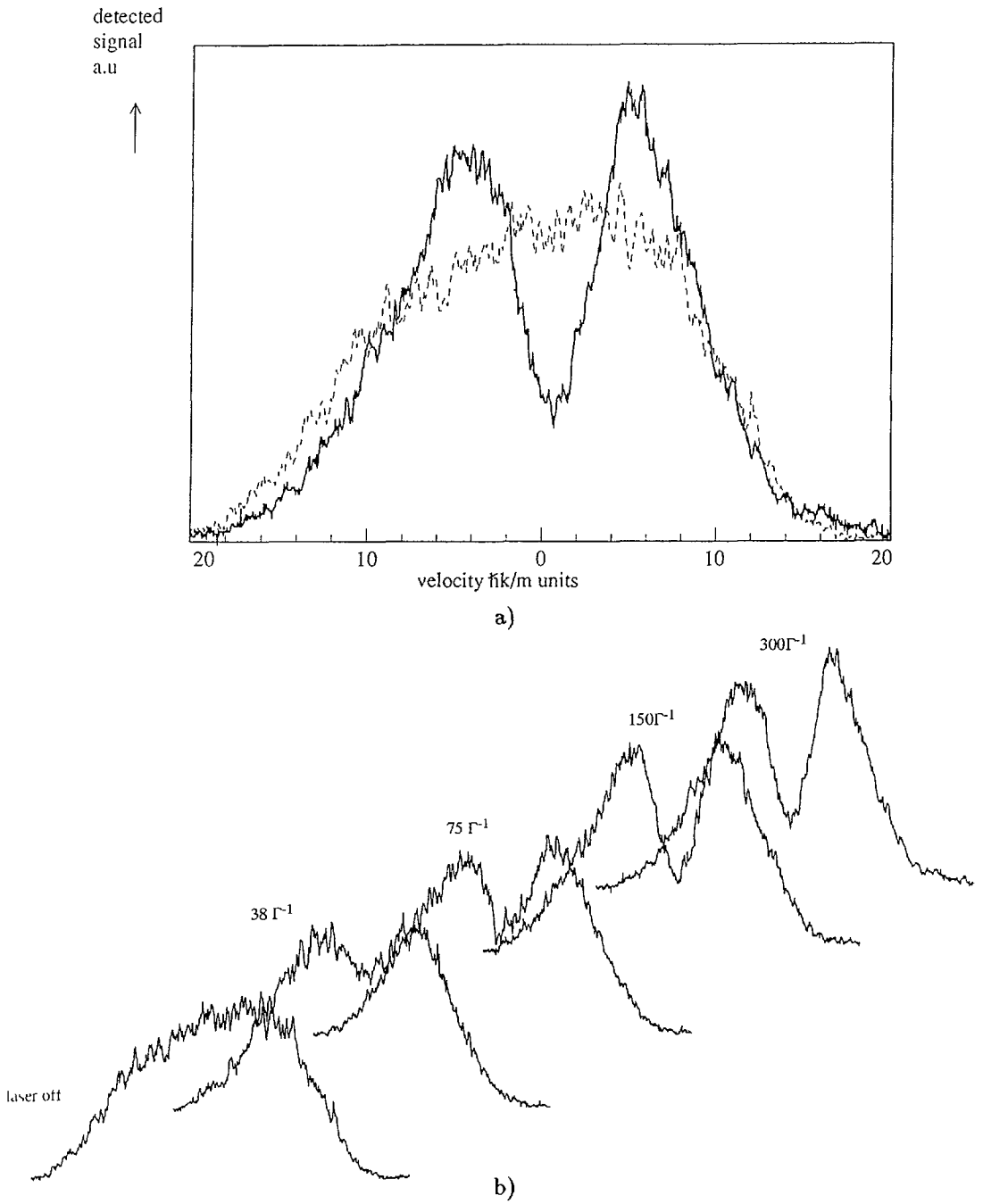

Fig. 8. — MASE for a negative detuning. a) presents the final velocity distribution after interaction with the lasers (solid line), in the presence of a transverse magnetic field, with values of the parameters (laser intensity, magnetic field, detuning) corresponding to those of figure 6. The hole around $v = 0$ is a clear signature of the MASE effect expelling the atoms off $v = 0$. This result was obtained after an interaction time of $300\Gamma^{-1}$ (30 μs). The dotted curve presents the initial distribution. b) Velocity distributions at intermediate times, obtained by masking a part of the transverse laser beam. It is clear that a steady state situation is not yet reached at $300\Gamma^{-1}$

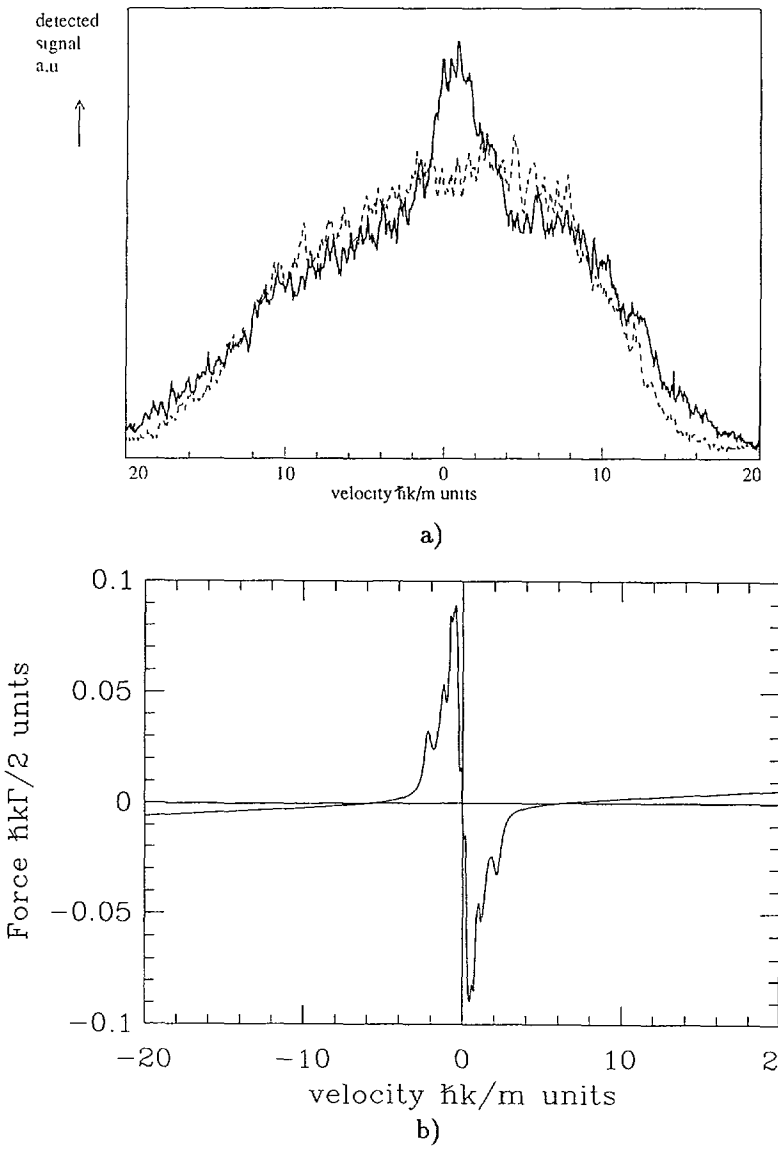

Fig. 9. — MASE for positive detuning. a) presents the velocity distribution after an interaction time of $300\Gamma^{-1}$. The parameters are: $\delta = +4.5\Gamma$; $\Omega_B = 0.077\Gamma$, $\Omega_L = 2.6\Gamma$. b) gives the result of the calculation of the force as a function of the velocity, for the parameters of figure 9a. It predicts a cooling around $v = 0$, observed in figure 9a and a heating in the wings, only slightly visible because the interaction time is not long enough. The dotted curve presents the initial distribution.

argument of section 2 then no longer applies, because the Zeeman term of the Hamiltonian cannot be considered as a perturbation. In this case, one can argue that the Larmor precession between the various ground state sublevels is large enough to prevent accumulation of atoms in g_+ by optical pumping. The $J_g = 1$ to $J_e = 1$ transition will then behave as an effective two level cycling transition. We then expect to observe Doppler cooling.

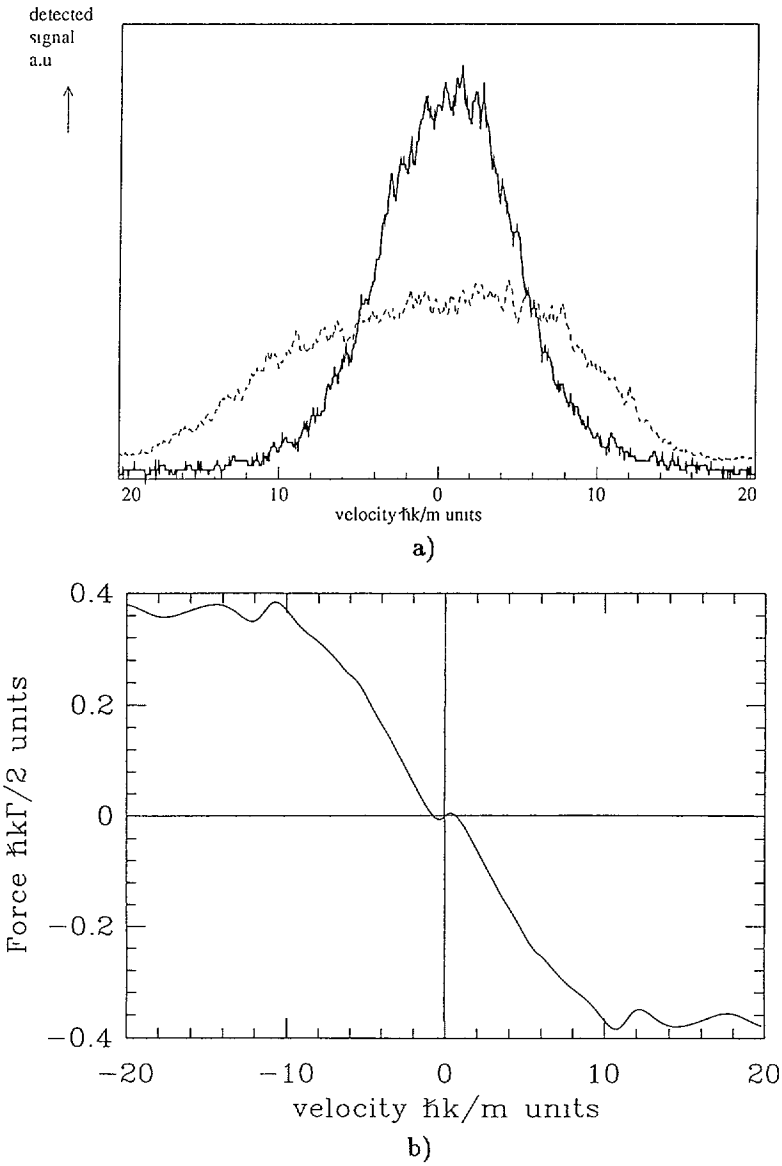

Fig. 10. — Large transverse magnetic field, and negative detuning. a) presents the final velocity distribution, in a situation where the Larmor frequency $\Omega_B(1.3\Gamma)$ is larger than the light-shifts ($\Omega_L = 2.4\Gamma$, $\delta = -1.13\Gamma$) so that the system behaves as a two level system. We indeed observe Doppler cooling. The dotted curve presents the initial distribution. b) Calculated average force (as calculated in 3.6).

Figure 10a presents a result supporting this picture, since a clear cooling is observed for negative detuning. This curve has been obtained with a Larmor frequency ($\Omega_B = 1.3\Gamma$) larger than the light shifts (of the order of 0.7Γ). Figure 10b presents the result of the calculation of section 3 for these values of parameters, and we see indeed a predicted cooling force with a characteristic evolution time ($65\Gamma^{-1}$) shorter than the interaction time.

4.3.2 *Longitudinal magnetic field.* — Coming back to a situation where the physical discussion of section 2 applies, we are now interested in the effect of a longitudinal magnetic field, applied along the direction of propagation of the laser (Oz) in addition to the transverse field. We can make a qualitative prediction by considering how figures 3 and 4 are modified. Ignoring the level g_- (we come back to the simplified 3 sublevels scheme of Sect. 3.2), we see that the effect of a longitudinal magnetic field is to displace g_+ with g_0 unaffected. If g_+ moves upwards by a quantity larger than the transverse Larmor frequency, the two sublevels remain always well separated, so that the magnetic precession at a node becomes negligible, and the force vanishes. For the opposite sign of the longitudinal field, g_+ moves downwards. A very interesting situation happens when g_+ crosses g_0 around the antinodes (Fig. 11a): we again have a Sisyphus effect, but now the magnetic precession happens at the bottom of the potential hills, and the Sisyphus is expected to cool instead of heating. We thus predict that for a longitudinal magnetic field with a well chosen orientation and magnitude, MASE can cool for a negative detuning, and its effect will just add to the usual Doppler cooling.

By applying a longitudinal magnetic field, we indeed observe cooling for a negative detuning. Figure 11c has been obtained for $\Omega_L = 2.4\Gamma$, $\delta = -0.94\Gamma$, and for a transverse magnetic field corresponding to a precession frequency $\Omega_B = 0.15\Gamma$. The longitudinal magnetic field is equal to -0.26 G, corresponding to a Zeeman shift of -0.45Γ for the level g_+. Figure 11b shows the calculated force as a function of the velocity. The shape of the curve clearly agrees with the interpretation of a cooling Sisyphus effect around $v = 0$, added to the standard Doppler cooling effect, acting on a wider range. We have also checked that for a reversed longitudinal magnetic field the velocity distribution is not affected by the laser beam, as predicted by the qualitative picture above as well as by the calculation that shows that the force is negligible.

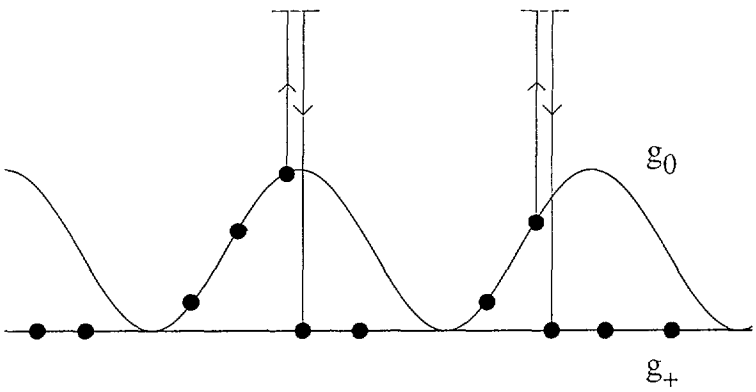

a)

Fig. 11. — MASE in the presence of a negative longitudinal field ($\Omega_L = 2.4\Gamma$; $\delta = -0.94\Gamma$; transverse magnetic field: $\Omega_B = 0.15\Gamma$; longitudinal magnetic field $B_{||} = -0.26$ G). a) Position of the ground state energy levels. In this situation the corresponding Sisyphus effect produces a cooling, for a negative detuning. b) Average force, calculated as explained in section 3.6. The structure around $v = 0$ corresponds to MASE, while the broader structure is the ordinary Doppler cooling. c) Velocity distribution after an interaction time of $300\Gamma^{-1}$ One clearly sees the central peak corresponding to MASE which now produces cooling. The dotted curve presents the initial distribution.

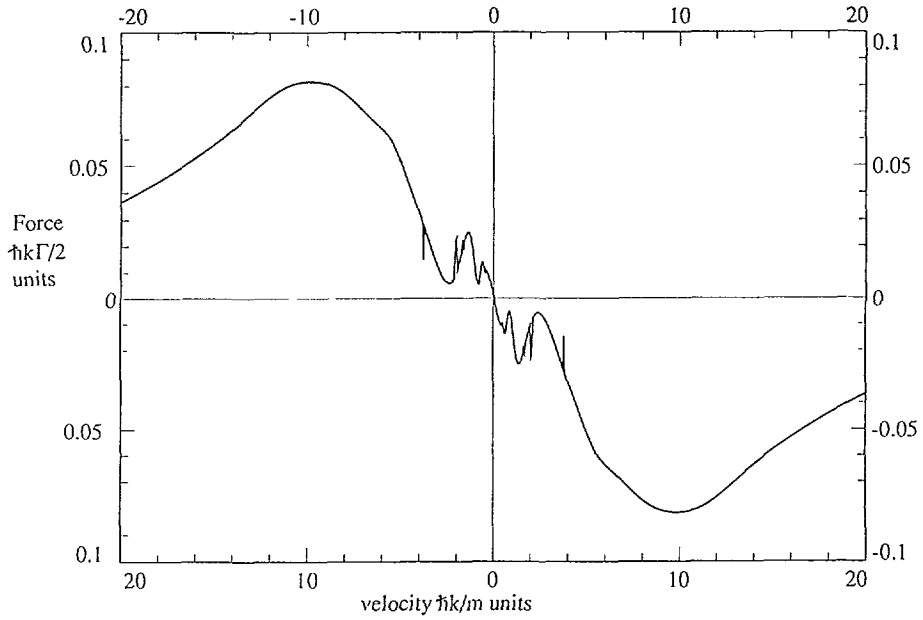

b)

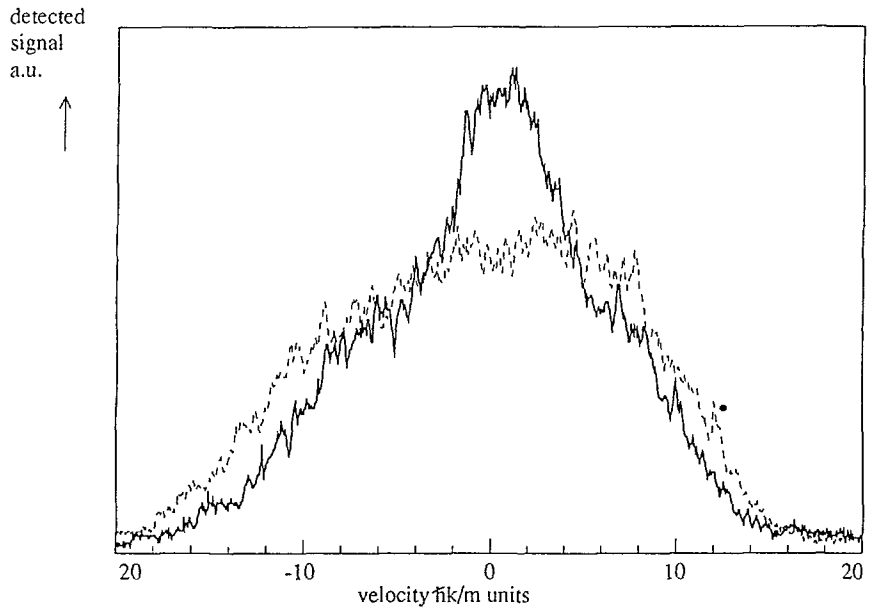

c)

Fig. 11. — (*continued*).

4.4 DISCUSSION. — We have presented several experimental results, agreeing with the physical pictures developed in section 2, and based on the existence of two effects: the standard Doppler cooling effect, and the Magnetically Assisted Sisyphus Effect. The respective signs

and weights of these effects are determined by the values of the various parameters (detuning, transverse magnetic field, longitudinal magnetic field). The qualitative predictions are in good agreement with the experimental observations and with the results of the semi-classical calculation of the force (as explained in Sect. 3).

We could now try to make a more quantitative analysis of the velocity distribution shape. In our experiments the interaction time is not long enough for the velocity distribution to reach a steady state, so that a precise comparison requires the calculation of the transient evolution. This evolution is governed by a Fokker-Planck type equation [25], for which we must know not only the average force calculated in section 3, but also the velocity diffusion coefficient. Such an approach would thus require the calculation of this coefficient, and the resolution of the corresponding Fokker-Planck equation. Such calculations are far from being trivial ([3]), and we present in the next section an alternative approach.

5. Full quantum treatment.

5.1 LIMITATIONS OF THE SEMI-CLASSICAL APPROACH. — The Fokker-Planck equation approach mentioned above is not only difficult from a computational point of view, but it becomes questionable when the one-photon recoil velocity $\hbar k/M$ is not small compared to the width of the velocity distribution. We are precisely in such a situation in the case of helium. Indeed, we currently achieve velocity distributions with widths less than 50 cm/s, while the one photon recoil velocity is 9.2 cm/s. It is thus legitimate to raise the question of a full quantum treatment, where the motion is quantized, so that the finite value of the one-photon recoil velocity is incorporated in the theory. This is what we are going to do in this section, by the use of Generalized Optical Bloch Equations (GOBE). We will also find another benefit to this approach: since the GOBE are ordinary differential equations, it is quite easy to numerically solve them in the transient regime, and we have thus a very efficient tool for describing the experimental results of section 4, which are not obtained in the steady state situation.

5.2 PRINCIPLE OF THE CALCULATION. — We have to find the time evolution of the density matrix elements:

$$\langle \alpha, m_\alpha, p | \rho | \alpha', m_{\alpha'}, p' \rangle = \rho_{\alpha, m_\alpha, \alpha', m_{\alpha'}}(p, p') \tag{5.1}$$

where α and α' may denote the ground state g as well as the excited state e, with magnetic sublevels m_α and $m_{\alpha'}$, and where p and p' are the atomic momentum components parallel to the laser beam. Here, we do not use the "momentum family" notation where a single momentum p labels a set of states which are coupled by absorption and stimulated emission of laser photons as in [26, 27]. This basis is not appropriate here because an infinite redistribution of photons between the counterpropagating σ^+ waves is allowed and may lead to unlimited atomic momentum transfer $p \to p + n\hbar k$ with arbitrary n [28]. Consequently, we also have to calculate density matrix elements which are off diagonal with respect to p. These elements describe a localization of the atom within the intensity gradient of the laser standing wave.

The GOBE for the $J_g = 1$ to $J_e = 1$ transition are implemented in several steps. First we write down all equations which do not involve momentum changes, i.e. which have the general form:

$$\frac{\mathrm{d}}{\mathrm{d}t}\rho(p, p') = \frac{1}{i\hbar}\left[H_0, \rho(p, p')\right] \tag{5.2}$$

([3]) Note that in order to be completely rigorous, the semi-classical approach would require to take into account the position dependence of the force and of the diffusion coefficient.

The momentum-independent part involves the internal energy H'_A (in the interaction representation with respect to the laser mode evolution), plus the Zeeman term V_B:

$$H'_A = -\sum_{m_e} |e, m_e, p\rangle\, \hbar\delta\, \langle e, m_e, p| \tag{5.3}$$

$$V_B = \sum_{\alpha, m_\alpha, p} |\alpha, m_\alpha, p\rangle\, \frac{g_\alpha \hbar \widetilde{\Omega_B}}{\sqrt{2}}\, \langle \alpha, m_\alpha + 1, p| \;+\; \text{h.c.}, \tag{5.4}$$

g_α being the Landé factor ([4]). Evaluating the commutators with H'_A and V_B, we obtain for example the corresponding evolution of the optical coherence $\langle g, 0, p|\rho|e, 1, p'\rangle$:

$$\begin{aligned}\frac{d}{dt}\langle g, 0, p|\rho|e, 1, p'\rangle = {} & i g_e \frac{\widetilde{\Omega_B}}{\sqrt{2}} \langle g, 0, p|\rho|e, 0, p'\rangle \\ & - i g_g \frac{\widetilde{\Omega_B}}{\sqrt{2}} [\langle g, 1, p|\rho|e, 1, p'\rangle + \langle g, -1, p|\rho|e, 1, p'\rangle] \\ & - i\delta \langle g, 0, p|\rho|e, 1, p'\rangle\end{aligned} \tag{5.5}$$

The contribution of the kinetic energy operator leaves the internal degrees of freedom invariant and we obtain:

$$\frac{d}{dt}\, \langle \alpha, m_\alpha, p|\, \rho\, |\alpha', m_{\alpha'}, p'\rangle = (2i\hbar m)^{-1}\, (p^2 - p'^2)\, \langle \alpha, m_\alpha, p|\, \rho\, |\alpha', m_{\alpha'}, p'\rangle \tag{5.6}$$

The part of the Hamiltonian which does involve momentum changes is simple since the atom-field interaction can change p and p' only by $\pm\, \hbar k$:

$$\begin{aligned}\frac{d}{dt}\, \langle g, m_g, p|\, \rho\, |e, m_e, p'\rangle = {} & \frac{i\Omega_L}{2} \\ & \left(\begin{array}{l} \displaystyle\sum_{m'_g} \delta_{m'_g+1, m_e} \left[\langle g, m_g, p|\, \rho\, |g, m'_g, p' + \hbar k\rangle + \langle g, m_g, p|\, \rho\, |g, m'_g, p' - \hbar k\rangle\right] \\ \displaystyle -\sum_{m'_e} \delta_{m_g+1, m'_e} \left[\langle e, m'_e, p + \hbar k|\, \rho\, |e, m_e, p'\rangle + \langle e, m'_e, p - \hbar k|\, \rho\, |e, m_e, p'\rangle\right] \end{array} \right)\end{aligned} \tag{5.7a}$$

$$\begin{aligned}\frac{d}{dt}\, \langle g, m_g, p|\, \rho\, |g, m'_g, p'\rangle = {} & \frac{i\Omega_L}{2} \\ & \left(\begin{array}{l} \displaystyle\sum_{m_e} \Big(\delta_{m'_g+1, m_e} \left[\langle g, m_g, p|\, \rho\, |e, m_e, p' + \hbar k\rangle + \langle g, m_g, p|\, \rho\, |e, m_e, p' - \hbar k\rangle\right] \\ \qquad - \delta_{m_g+1, m_e} \left[\langle e, m_e, p + \hbar k|\, \rho\, |e, m'_g, p'\rangle + \langle e, m_e, p - \hbar k|\, \rho\, |e, m'_g, p'\rangle\right] \Big) \end{array} \right)\end{aligned} \tag{5.7b}$$

$$\begin{aligned}\frac{d}{dt}\, \langle e, m_e, p|\, \rho\, |e, m'_e, p'\rangle = {} & \frac{i\Omega_L}{2} \\ & \left(\begin{array}{l} \displaystyle\sum_{m_g} \Big(\delta_{m_g+1, m_e} \left[\langle g, m_g, p + \hbar k|\, \rho\, |e, m'_e, p' + \hbar k\rangle + \langle g, m_g, p - \hbar k|\, \rho\, |e, m'_e, p'\rangle\right] \\ \qquad - \delta_{m_g+1, m'_e} \left[\langle e, m_e, p|\, \rho\, |g, m_g, p' + \hbar k\rangle + \langle e, m_e, p - \hbar k|\, \rho\, |g, m_g, p' - \hbar k\rangle\right] \Big) \end{array} \right)\end{aligned} \tag{5.7c}$$

([4]) With this notation, where the Landé factor g_α appears explicitly, the parameter Ω_B of equation (3.4) is equal to $g_g \widetilde{\Omega_B}$.

After having collected all the terms from the Hamiltonian evolution, we add all the contributions due to the decay of the excited state amplitudes:

$$\frac{\mathrm{d}}{\mathrm{d}t}\langle \mathrm{g}, m_\mathrm{g}, p|\,\rho\,|\mathrm{e}, m_\mathrm{e}, p'\rangle = -\frac{\Gamma}{2}\langle \mathrm{g}, m_\mathrm{g}, p|\,\rho\,|\mathrm{e}, m_\mathrm{e}, p'\rangle \tag{5.8a}$$

$$\frac{\mathrm{d}}{\mathrm{d}t}\langle \mathrm{e}, m_\mathrm{e}, p|\,\rho\,|\mathrm{e}, m'_\mathrm{e}, p'\rangle = -\Gamma\langle \mathrm{e}, m_\mathrm{e}, p|\,\rho\,|\mathrm{e}, m'_\mathrm{e}, p'\rangle \tag{5.8b}$$

For the repopulation of the ground state one has to take into account the momentum change due to the z component of the fluorescence photon recoil (straightforward generalization of the calculation of [27]). We derive after tracing over the transverse momentum components:

$$\frac{\mathrm{d}}{\mathrm{d}t}\langle \mathrm{g}, m_\mathrm{g}, p|\,\rho\,|\mathrm{g}, m'_\mathrm{g}, p'\rangle$$

$$= \Gamma \sum_{q=-1,0,+1} \int_{-\hbar k}^{\hbar k} \mathrm{d}p'' N_q(p'')\langle \mathrm{e}, m_\mathrm{e}, p+p''|\,\rho\,|\mathrm{e}, m'_\mathrm{e}, p'+p''\rangle C^{m_\mathrm{e}}_{m_\mathrm{g},q} C^{m'_\mathrm{e}}_{m'_\mathrm{g},q} \tag{5.9a}$$

$$\text{with}\quad N_{\pm 1}(p) = \frac{3}{8\hbar k}\left(1+\left(\frac{p}{\hbar k}\right)^2\right)\quad\text{and}\quad N_0(p) = \frac{3}{4\hbar k}\left(1-\left(\frac{p}{\hbar k}\right)^2\right) \tag{5.9b}$$

$C^{m_\mathrm{e}}_{m_\mathrm{g},q} C^{m'_\mathrm{e}}_{m'_\mathrm{g},q}$ being the product of the Clebsch-Gordan coefficients. Adding all these contributions gives the GOBE. By integration on a suitable momentum grid by ordinary differential equation solvers, we obtain the density operator $\rho(t)$ at any time. Tracing over all the internal degrees of freedom, we get the momentum distribution at time t:

$$W(p,t) = \sum_{\alpha, m_\alpha} \langle \alpha, m_\alpha, p|\,\rho(t)\,|\alpha, m_\alpha, p\rangle \tag{5.10}$$

5.3 RESULTS AND DISCUSSION. — The GOBE obtained in section 5.2 are integrated step by step, using a Runge Kutta method (step $\Gamma^{-1}/10$). For a momentum grid of 80 points ($\Delta p = 40\hbar k$) and 6 internal states, the density matrix has $480^2 = 230400$ elements. Symmetry considerations cannot be used to reduce this number since the initial momentum profiles are not symmetrical. The initial distribution chosen for the calculation is a diagonal statistical mixture: the ground state sublevels are equally populated, and the excited states are empty, the initial momentum distribution reproducing the distribution obtained experimentally in the absence of light.

A result of such a calculation is shown in figure 12. We have taken the same parameters as in figure 8. The momentum distribution has been plotted for several interaction times, differing by $50\Gamma^{-1}$

The sequence of calculated profiles render a reasonable account of the measured profiles. In particular, it shows a fast evolution around $v = 0$, while the evolution in the wings is very slow ([5]). Note a singularity in the initial evolution, specially striking in the wings. We have checked that this takes place in a few Γ^{-1}, that is to say that it is due to the exchange of the first photons. In fact, it can be interpreted as the momentum exchange happening during the initial optical pumping that redistributes the atomic population (initially equally distributed) between the various Zeeman sublevels. An analogous similar feature was already noticed for the Mechanical Hanle Effect [15].

([5]) At interaction times much longer than in the experiment, this calculation shows a slow narrowing of the profile in the wings at a time scale of the order of $1000\Gamma^{-1}$

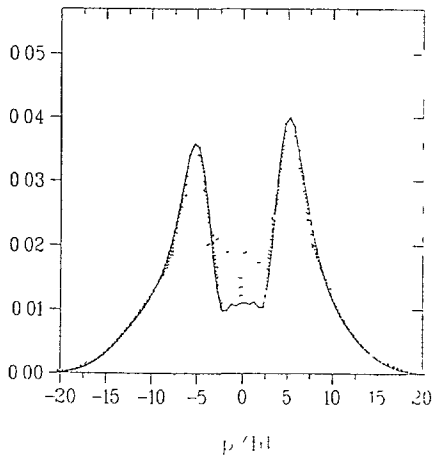

Fig. 12. — Numerical resolution of the Generalized Optical Bloch Equation for the parameters of figure 6. The momentum distribution has been plotted for several interaction times differing by $50\Gamma^{-1}$. The two bumps are centered at velocities $v_1 = \pm\ 5.3\hbar k/M$. The shape of the curve for various evolution time is very similar to the experimental results of figure 8b.

6. Conclusion.

We have presented in this paper a study of laser cooling in a standing wave in the presence of a transverse magnetic field (Magnetically Assisted Sisyphus Effect) for a $J_g = 1$ to $J_e = 1$ transition. In this situation, MASE has an effect opposed to the usual Doppler cooling effect, i.e. it is heating for a negative detuning (below resonance). The two effects play a role, but they have different velocity dependences: Sisyphus cooling is more efficient than Doppler cooling on a narrower velocity range around zero, which corresponds to larger friction coefficients and thus to shorter evolution times for the velocity distribution. At large velocities, Doppler cooling dominates. The result is a rich variety of behaviors, depending on the various parameters (laser intensity and detuning, magnetic field, interaction time). For instance, in the case of a negative detuning, one has a bistable force. By adding a longitudinal magnetic field, one can reverse MASE, without changing Doppler cooling, so that the two effects add up instead of competing.

Experimental results corresponding to these various situations support the qualitative predictions. In order to interpret these results more quantitatively, we have used several theoretical approaches. First, we have shown how it is possible to calculate a velocity dependent average force, by use of a continued fraction expansion of the solution of optical Bloch equations. Such a treatment explains various features: position of the bumps, different time constants. In order to give a more complete description of the profile and of the transient time evolution of the velocity distribution, we have then used a second theoretical treatment, in which the atomic motion is quantized. In the case of helium, this approach is also motivated by the fact that the one photon recoil velocity $\hbar k/M$ is not very small compared to the velocity distribution width.

The results presented in this paper could be generalized along several lines. First, for any transition with the same angular momentum in the ground and in the excited states, we expect similar qualitative behaviors. Second, it is interesting to note that the full quantum treatment

may be interesting even in situations in which a semi-classical treatment is still valid, when one wants a detailed description of the velocity distribution, incorporating the transient evolution and/or the diffusion associated (in the semi-classical description) to the fluctuations of the force around its steady state value. The calculation is in principle very simple, since the GOBE are ordinary first order differential equations. However, the numerical integration may become a problem if the density matrix has too many elements, that exceed the size of the computer memory. This happens because of the quantization of the linear momentum, and the problem is specially critical if one considers a problem in 2 or 3 dimensions. In such cases, the recently developed quantum Monte-Carlo methods [29, 30] may provide another convenient way of computing the exact evolution of the velocity distribution.

Acknowledgements.

Hartmut Wallis acknowledges the kind hospitality of the ENS group and support by the E.E.C. Christoph Gerz wishes to thank the Deutsche Forschungsgemeinschaft for its support. This work was supported by D.R.E.T.

References

[1] Lett P., Watts R., Westbrook C., Phillips W.D., Gould P. and Metcalf H., *Phys. Rev. Lett.* **61** (1988) 169.

[2] Dalibard J., Salomon C., Aspect A., Arimondo E., Kaiser R., Vansteenkiste N. and Cohen-Tannoudji C., in proceedings of the 11th conference on Atomic Physics, S. Haroche, J-C. Gay and G. Grynberg Eds. (World Scientific, Singapore, 1989).

[3] Shevy Y., Weiss D.S. and Chu S., in Proceedings of the conference on spin polarized quantum systems, S. Stringari Eds. (World Scientific, Singapore, 1989);
Shevy Y., Weiss D.S., Ungar P.J. and Chu S., *Phys. Rev. Lett.* **62** (1989) 1118.

[4] Chu S., Weiss D.S., Shevy Y. and Ungar P.J., in proceedings of the 11th conference on Atomic Physics, S. Haroche, J.C. Gay and G. Grynberg Eds. (World Scientific, Singapore, 1989).

[5] Dalibard J. and Cohen-Tannoudji C., *J.O.S.A.* **B6** (1989) 2023.

[6] Ungar P.J., Weiss D.S., Riis E. and Chu S., *J.O.S.A.* **B6** (1989) 2058.

[7] Dalibard J. and Cohen-Tannoudji C., *J.O.S.A.* **B2** (1985) 1707.

[8] Sheehy B., Shang S.Q., van der Straten P., Hatamian S. and Metcalf H., *Phys. Rev. Lett.* **64** (1990) 858.

[9] Weiss D.S., Riis E., Shevy Y., Ungar P.J. and Chu S., *J.O.S.A.* **B6** (1989) 2072.

[10] Aspect A., Emile O., Gerz C., Kaiser R., Vansteenkiste N., Wallis H. and Cohen-Tannoudji C., Proceedings of the Enrico Fermi course on Laser Manipulation of Atoms and Ions (Varenna, 1991).

[11] Shang S.Q., Sheehy B., van der Straten P. and Metcalf H., *Phys. Rev. Lett.* **65** (1990) 317.

[12] Metcalf H., Proceedings of the Enrico Fermi course on Laser Manipulation of Atoms and Ions, (Varenna, 1991).

[13] Nienhuis G., van der Straten P. and Shang S.Q., *Phys. Rev.* **A 44** (1991) 462.

[14] Valentin C., Gagné M.C., Yu J. and Pillet P., *Europhys. Lett.* **17** (1991) 133.

[15] Kaiser R., Vansteenkiste N., Aspect A., Arimondo E. and Cohen-Tannoudji C., *Z. Phys. D.* **18** (1991) 17.

[16] Suominen K.A., *Opt. Commun.* **93** (1992) 126; Ph.D. Thesis, Helsinki (1992).

[17] Cohen-Tannoudji C., Les Houches Course XXX (1990), Part. I, Chap. 2., J. Dalibard, J.M. Raimond and J. Zinn-Justin Eds. (Elsevier Science Publishers B.V., 1992).

[18] Minogin V.G. and Serimaa O.T., *Opt. Commun.* **30** (1979) 373.
[19] Aspect A., Arimondo E., Kaiser R., Vansteenkiste N. and Cohen-Tannoudji C., *Phys. Rev. Lett.* **61** (1988) 826.
[20] Aspect A., Vansteenkiste N., Kaiser R., Haberland H. and Karrais M., *Chem. Phys.* **145** (1990) 307.
[21] Vansteenkiste N., Gerz C., Kaiser R., Hollberg L., Salomon Ch. and Aspect A., *J. Phys. II France* **1** (1991) 1407.
[22] Bigelow N.P. and Prentiss M.G., *Phys. Rev. Lett.* **65** (1990) 555.
[23] Tollett J.J., Chen J., Story J.G., Ritchie N.W.M., Bradley C.C. and Hulet R.G., *Phys. Rev. Lett.* **65** (1990) 559.
[24] Garraway B.M. and Stenholm S., *Phys. Rev.* **A45** (1992) 364.
[25] Part I, chap. 5 of reference [17].
[26] Aspect A., Arimondo E., Kaiser R., Vansteenkiste N. and Cohen-Tannoudji C., *J.O.S.A.* **B6** (1989) 2112.
[27] Castin Y., Wallis H. and Dalibard J., *J.O.S.A.* **B6** (1989) 2046.
[28] Castin Y., Dalibard J. and Cohen-Tannoudji C., Light induced kinetic effects on atoms and molecules, L. Moi, C. Gozzini, E. Arimondo, F. Strumia Eds. (Ets. Editrice, Pisa, 1991).
[29] Dalibard J., Castin Y. and Mølmer K., *Phys. Rev. Lett.* **68** (1992) 580.
[30] Cohen-Tannoudji C., Bardou F. and Aspect A., Proceedings of the Tenth International Conference on Laser spectroscopy (Font-Romeu), M. Ducloy, E. Giacobino, G. Camy Eds. (World Scientific, 1992).